

THERMAL BEHAVIOR, CRYSTALLIZATION, AND MAGNETIC PROPERTIES OF $\text{Fe}_{81}\text{Zr}_5\text{Nb}_4\text{B}_{10}$ AND $\text{Fe}_{40.5}\text{Co}_{40.5}\text{Zr}_5\text{Nb}_4\text{B}_{10}$ AMORPHOUS ALLOYS

B. Zuo,^{1,2} J. H. Wang,¹ Z. Q. Song,¹ X. J. Xue,¹ and X. N. Wang²

Translated from *Metallovedenie i Termicheskaya Obrabotka Metallov*, No. 4, pp. 51 – 55, April, 2020.

Amorphous alloys $\text{Fe}_{81}\text{Zr}_5\text{Nb}_4\text{B}_{10}$ and $\text{Fe}_{40.5}\text{Co}_{40.5}\text{Zr}_5\text{Nb}_4\text{B}_{10}$ obtained by melt spinning and subjected to annealing at different temperatures are studied. The activation energy of crystallization of the alloys is determined for different heating rates. It is shown that the primary product of crystallization of amorphous alloy $\text{Fe}_{81}\text{Zr}_5\text{Nb}_4\text{B}_{10}$ is an α -Fe phase and a phase with a structure of type α -Mn. In the presence of cobalt, the primary product of crystallization of alloy $\text{Fe}_{40.5}\text{Co}_{40.5}\text{Zr}_5\text{Nb}_4\text{B}_{10}$ is an α -Fe(Co) phase. The difference in the crystallization products affects the coercivity.

Key words: amorphous alloys, transformations under heating, thermal analysis, magnetic properties.

INTRODUCTION

Amorphous Fe-base soft magnetic alloys have been studied long enough [1 – 3] and have wide specific application, for example, in transformer cores and magnetic sensors. The crystallization kinetics of Fe-base amorphous alloys is an important subject of research, which especially concerns analysis of the activation energy of crystallization [4]. Isoconversional methods of assessing the activation energy of crystallization processes may be classified conventionally into two categories, i.e., isothermal and non-isothermal ones [5]. However, amorphous iron-base alloys are commonly annealed under non-isothermal conditions. Therefore, it seems expedient to calculate the activation energy of crystallization of these alloys in terms of non-isothermal crystallization kinetics.

Quite a number of methods have been created for calculating the activation energy of crystallization processes within non-isothermal kinetics, for example, the methods of Ozawa [6], Boswell, Starink [8] and Kissinger [6, 9]. Kissinger's method is used the most frequently for calculating the activation energy of crystallization of Fe-base amorphous alloys [10 – 14].

We should mention three groups of amorphous and nanocrystalline soft magnetic alloys based on iron, i.e.,

FINEMET [Fe – Cu – M – Si – B (M = Nb, Mo, W, Ta)], NANODERM [Fe – M – B (M = Zr, Hf, Nb)] and HITPERM [(Fe, Co) – M – B (M = Zr, Hf, Nb)]. The aim of the present work was to study the magnetic properties, the thermal behavior, and the processes of crystallization of alloys $\text{Fe}_{81}\text{Zr}_5\text{Nb}_4\text{B}_{10}$ (NANODERM type) and $\text{Fe}_{40.5}\text{Co}_{40.5}\text{Zr}_5\text{Nb}_4\text{B}_{10}$ (HITPERM type).

METHODS OF STUDY

Amorphous ribbons from alloys $\text{Fe}_{81}\text{Zr}_5\text{Nb}_4\text{B}_{10}$ and $\text{Fe}_{40.5}\text{Co}_{40.5}\text{Zr}_5\text{Nb}_4\text{B}_{10}$ were obtained by melt spinning in a device with a copper wheel rotating at a surface speed of 30 m/sec. The ribbons were annealed at 573, 823, 873, 943 and 1023 K for 40 min. The differential thermal analysis (DTA) was conducted using an STA 449F5 device for synchronous thermal analysis at different heating rates (7, 10, 15, 20 and 30 K/min). The structure of the alloys was studied using a D/max 2500/PC x-ray diffractometer in copper K_α radiation with wavelength $\lambda = 1.5406 \text{ \AA}$ and a JEM-2100E transmission electron microscope (TEM) at an accelerating voltage of 200 kV. The magnetic properties were measured using a Lake Shore M7407 vibrating sample magnetometer.

RESULTS AND DISCUSSION

Figure 1 presents the DTA curves for quenched alloys $\text{Fe}_{81}\text{Zr}_5\text{Nb}_4\text{B}_{10}$ (a) and $\text{Fe}_{40.5}\text{Co}_{40.5}\text{Zr}_5\text{Nb}_4\text{B}_{10}$ (b) at heating

¹ National Demonstration Center for Experimental Physics Education, Jilin Normal University, Jilin, China (e-mail: zuobin1027@163.com).

² Key Laboratory of Functional Materials Physics and Chemistry of the Ministry of Education, Jilin University, Jilin, China.

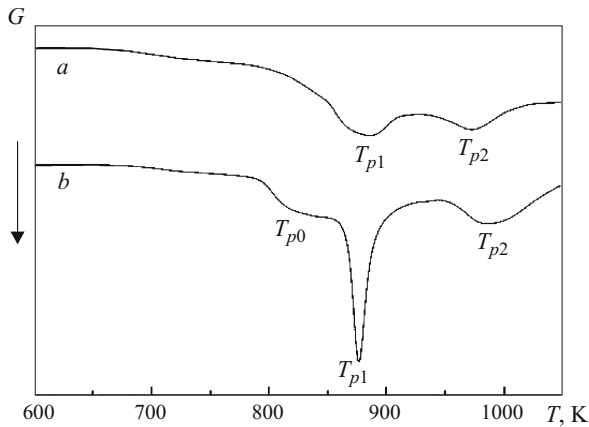


Fig. 1. DTA curves for alloys $\text{Fe}_{81}\text{Zr}_5\text{Nb}_4\text{B}_{10}$ (a) and $\text{Fe}_{40.5}\text{Co}_{40.5}\text{Zr}_5\text{Nb}_4\text{B}_{10}$ (b) at heating rate 10 K/min (G is the thermal effect).

rate 10 K/min. The heating curves of quenched alloy $\text{Fe}_{81}\text{Zr}_5\text{Nb}_4\text{B}_{10}$ have two exothermic peaks; the curves of quenched alloy $\text{Fe}_{40.5}\text{Co}_{40.5}\text{Zr}_5\text{Nb}_4\text{B}_{10}$ have three exothermic peaks.

Figure 2 presents the x-ray diffraction patterns for alloys $\text{Fe}_{81}\text{Zr}_5\text{Nb}_4\text{B}_{10}$ and $\text{Fe}_{40.5}\text{Co}_{40.5}\text{Zr}_5\text{Nb}_4\text{B}_{10}$ quenched and annealed at different temperatures. The diffraction patterns of the quenched alloys do not have peaks corresponding to crystalline phases, which reflects amorphous condition of both alloys after the quenching. After the annealing at 573 K the structure of the alloys remains amorphous. After the annealing at 873 K the $\text{Fe}_{81}\text{Zr}_5\text{Nb}_4\text{B}_{10}$ alloy contains crystals of phase $\alpha\text{-Fe}$ and a phase of type $\alpha\text{-Mn}$. It is known that $\alpha\text{-Mn}$ is a metastable phase [15 – 17]. With growth of the annealing temperature the $\alpha\text{-Mn}$ -type phase disappears giving way to an $\alpha\text{-Fe}$ solid solution. The two exothermic peaks on the DTA curve correspond to formation of $\alpha\text{-Fe}$ and $\alpha\text{-Mn}$ -type phases and to formation of a solid solution of $\alpha\text{-Fe}$, respec-

tively. The $\text{Fe}_{40.5}\text{Co}_{40.5}\text{Zr}_5\text{Nb}_4\text{B}_{10}$ alloy contains only an $\alpha\text{-Fe}(\text{Co})$ phase at the temperatures below 943 K. After the annealing at 1023 K, the alloy contains ZrNb and NbB phases. In the range between T_{p0} and T_{p1} the alloy has no other phase except $\alpha\text{-Fe}(\text{Co})$. It can be assumed that the temperature T_{p0} corresponds to the pre-crystallization effect [18], the temperature T_{p1} corresponds to formation of phase $\alpha\text{-Fe}(\text{Co})$, and the temperature T_{p2} corresponds to formation of phases ZrNb and NbB.

Figure 3 presents the microstructure (TEM) of alloys $\text{Fe}_{81}\text{Zr}_5\text{Nb}_4\text{B}_{10}$ (a) and $\text{Fe}_{40.5}\text{Co}_{40.5}\text{Zr}_5\text{Nb}_4\text{B}_{10}$ (b) after the annealing at 873 K. It can be seen from Fig. 3a that the structure of the alloy also contains fine inclusions of an irregular shape. The electron diffraction pattern shows reflections from planes (321) and (400) of an $\alpha\text{-Mn}$ -type phase with interplane distances 0.235 and 0.220 nm, respectively. Figure 3b presents inclusions of spherical particles; in this case, the electron diffraction pattern exhibits reflections from planes (110) and (200) of phase $\alpha\text{-Fe}(\text{Co})$ with interplane distances 0.201 and 0.1420 nm, respectively. The authors of [15] assume that the transformation of a $\alpha\text{-Mn}$ -type phase from amorphous condition into a crystalline one may occur easily due to diffusion of atoms to a relatively short distance. In accordance with the results described in [15], [17] the atoms of B, Zr and Nb are surrounded by Fe atoms and form a phase of type $\alpha\text{-Mn}$. When the $\alpha\text{-Mn}$ phase disappears, the atoms of B, Zr and Nb also dissolve in the crystal lattice of $\alpha\text{-Fe}$ yielding an $\alpha\text{-Fe}$ solid solution. In the $\text{Fe}_{40.5}\text{Co}_{40.5}\text{Zr}_5\text{Nb}_4\text{B}_{10}$ alloy, the negative heat of mixing of the amorphous alloy increases with the growth in the content of Co [19], and the Co atoms tend to dissolve in the crystal lattice of Fe in the heat treatment process. This is accompanied by full rearrangement of the atoms. The Zr, Nb and B elements are present in the residual amorphous phase during the crystallization of the alloy and precipitate in the form of phases ZrNb and NbB at 1023 K.

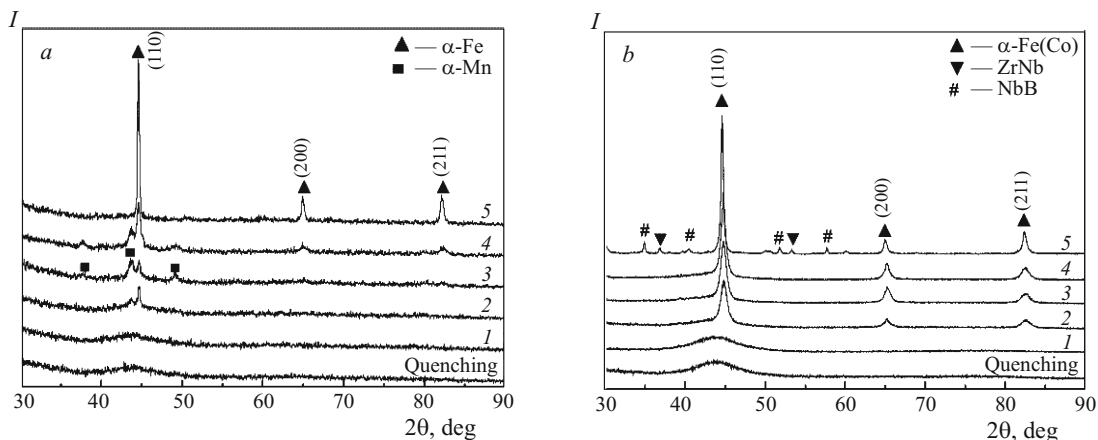


Fig. 2. Diffraction patterns for $\text{Fe}_{81}\text{Zr}_5\text{Nb}_4\text{B}_{10}$ (a) and $\text{Fe}_{40.5}\text{Co}_{40.5}\text{Zr}_5\text{Nb}_4\text{B}_{10}$ (b) after quenching and annealing at different temperatures: 1) 573 K; 2) 823 K; 3) 873 K; 4) 943 K; 5) 1023 K.

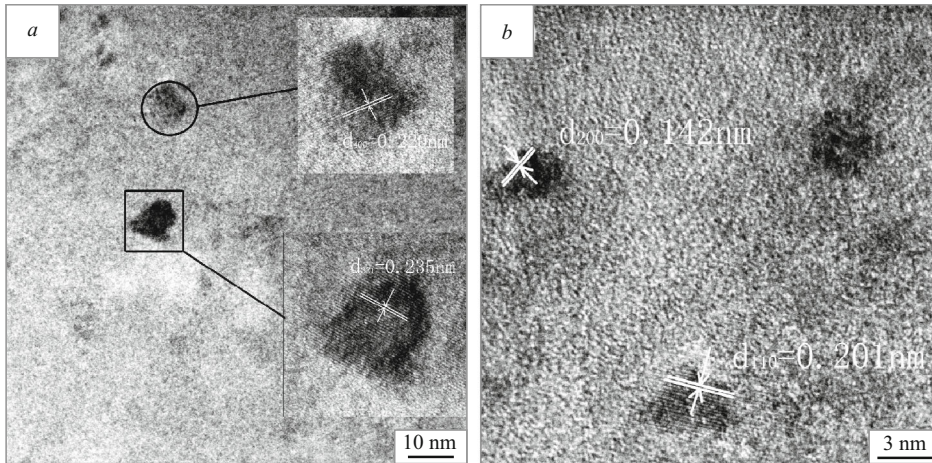


Fig. 3. Microstructure (TEM) of alloys $\text{Fe}_{81}\text{Zr}_5\text{Nb}_4\text{B}_{10}$ (a) and $\text{Fe}_{40.5}\text{Co}_{40.5}\text{Zr}_5\text{Nb}_4\text{B}_{10}$ (b) after annealing at 873 K.

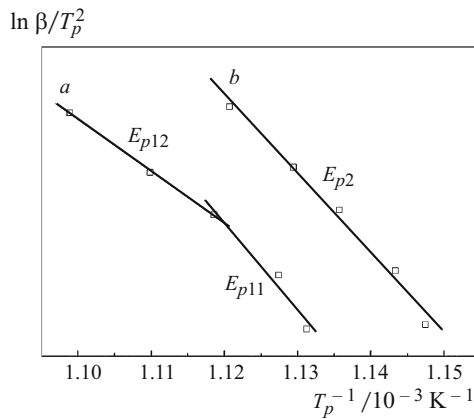


Fig. 4. Kissinger's dependences of alloys $\text{Fe}_{81}\text{Zr}_5\text{Nb}_4\text{B}_{10}$ (a) and $\text{Fe}_{40.5}\text{Co}_{40.5}\text{Zr}_5\text{Nb}_4\text{B}_{10}$ (b) for temperatures T_{p1} .

Thus, the processes of crystallization of the two alloys differs, which presents substantial interest. To understand the special features of crystallization, we determined the thermal characteristics of these alloys. The temperatures of the crystallization peaks T_{p1} are given in Table 1 for quenched alloys $\text{Fe}_{81}\text{Zr}_5\text{Nb}_4\text{B}_{10}$ and $\text{Fe}_{40.5}\text{Co}_{40.5}\text{Zr}_5\text{Nb}_4\text{B}_{10}$ heated at different rates.

The activation energy E of crystallization for the first peak T_p was calculated from Kissinger's equation [9] by plotting $\ln(V/T^2)$ as a function of $1/T$ (a straight line with slope E/R), where R is the gas constant, V is the heating rate in K/min, and T is the specific absolute temperature of the

crystallization peak T_{p1} . Kissinger's dependences for crystallization peaks T_{p1} of alloys $\text{Fe}_{81}\text{Zr}_5\text{Nb}_4\text{B}_{10}$ and $\text{Fe}_{40.5}\text{Co}_{40.5}\text{Zr}_5\text{Nb}_4\text{B}_{10}$ are given in Fig. 4. For the amorphous alloy $\text{Fe}_{81}\text{Zr}_5\text{Nb}_4\text{B}_{10}$ the critical heating rate is $V_{cr} = 15$ K/min. Kissinger's plot is divided into two regions with different slopes. The activation energy of the crystallization process $E_{p11} = 464.9$ kJ/mole for the heating rates of 7–15 K/min and $E_{p12} = 278.5$ kJ/mole for the heating rates of 15–30 K/min, which corresponds to formation of two different crystallization products. The barrier of nucleation of the α -Mn-type phase is higher than that of the α -Fe phase [20]. The value of E_{p11} corresponds to nucleation of the α -Mn-type phase, the value of E_{p12} corresponds to nucleation of the α -Fe phase. For the amorphous alloy $\text{Fe}_{40.5}\text{Co}_{40.5}\text{Zr}_5\text{Nb}_4\text{B}_{10}$ the value of $E_{p12} = 424.4$ kJ/mole.

The dependence of the coercivity H_c of quenched alloys $\text{Fe}_{81}\text{Zr}_5\text{Nb}_4\text{B}_{10}$ (a) and $\text{Fe}_{40.5}\text{Co}_{40.5}\text{Zr}_5\text{Nb}_4\text{B}_{10}$ (b) on the annealing temperature is presented in Fig. 5. It can be seen that the values of the coercivity of the two alloys differ significantly depending on the annealing temperature. For the $\text{Fe}_{81}\text{Zr}_5\text{Nb}_4\text{B}_{10}$ alloy the variation of H_c is inconsiderable up to 823 K. However, at 973 K the coercivity jumps to a maximum value. The insert in Fig. 5a presents the temperature dependence of H_c of alloy $\text{Fe}_{81}\text{Zr}_5\text{Nb}_4\text{B}_{10}$ in quenched condition and after annealing at 573, 973 and 1023 K. The lowering of H_c with growth of the temperature of the alloy quenched and annealed at 823 and 1023 is explainable by the thermal motion of atoms. The temperature dependence of H_c of the $\text{Fe}_{81}\text{Zr}_5\text{Nb}_4\text{B}_{10}$ alloy annealed at 873 K differs sub-

TABLE 1. Temperatures of Crystallization Peaks T_{p1} for Quenched Alloys $\text{Fe}_{81}\text{Zr}_5\text{Nb}_4\text{B}_{10}$ and $\text{Fe}_{40.5}\text{Co}_{40.5}\text{Zr}_5\text{Nb}_4\text{B}_{10}$ after Heating at Different Rates

| Alloy | T_{p1} , K, at heating rate, K/min | | | | |
|---|--------------------------------------|-------|-------|-------|-------|
| | 7 | 10 | 15 | 20 | 30 |
| $\text{Fe}_{81}\text{Zr}_5\text{Nb}_4\text{B}_{10}$ | 884.1 | 887.0 | 894.1 | 900.9 | 910.2 |
| $\text{Fe}_{40.5}\text{Co}_{40.5}\text{Zr}_5\text{Nb}_4\text{B}_{10}$ | 871.5 | 874.6 | 880.5 | 885.4 | 892.3 |

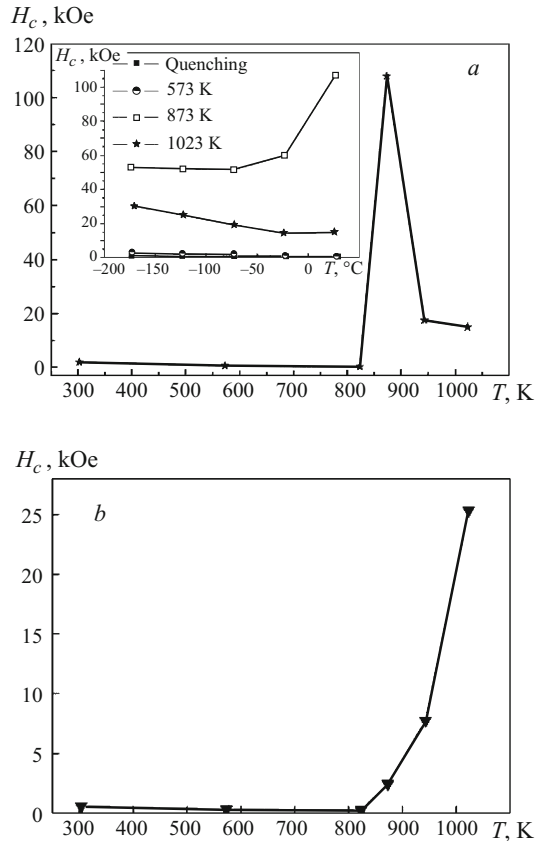


Fig. 5. Coercivity of alloys $\text{Fe}_{81}\text{Zr}_5\text{Nb}_4\text{B}_{10}$ (a) and $\text{Fe}_{40.5}\text{Co}_{40.5}\text{Zr}_5\text{Nb}_4\text{B}_{10}$ (b) as a function of the annealing temperature (the insert in Fig. 5a presents the temperature dependences of the coercivity of the alloys quenched and annealed at 573, 873 and 1023 K).

stantially from the temperature dependence of the alloy annealed at the other temperatures. At the low temperatures the variation of H_c of the alloy is determined primarily by the exchange coupling between crystallites, which mostly depends on the Curie temperature of the amorphous phase [21]. The fast decrease of H_c in the range from 300 K (about 30°C) to 200 K (−73°C) indicates the presence of a retained amorphous phase with a lower Curie temperature. In the range from 200 K (−73°C) to 100 K (−173°C) the coercivity remains virtually unchanged and preserves a higher value, which is connected with the presence of an α -Mn-type phase in the structure of the alloy. The temperature dependence of H_c shows that the elevation of the magnetic rigidity is connected with the lower Curie temperature of the amorphous phase and with the presence of an α -Mn-type phase in the structure, which has also been detected for alloy $\text{Fe}_{81}\text{Zr}_3\text{Nb}_9\text{B}_{10}$ [22]. The value of H_c in alloy $\text{Fe}_{40.5}\text{Co}_{40.5}\text{Zr}_5\text{Nb}_4\text{B}_{10}$ first decreases and then grows with the annealing temperature. The initial lowering of the coercivity occurs due to stress relaxation under the annealing, and the subsequent slow elevation is caused by growth in the

volume fraction of phase α -Fe(Co) in the structure of the alloy.

CONCLUSIONS

The results of our study of the process of crystallization, of the structure, and of the magnetic properties of amorphous alloys $\text{Fe}_{81}\text{Zr}_5\text{Nb}_4\text{B}_{10}$ and $\text{Fe}_{40.5}\text{Co}_{40.5}\text{Zr}_5\text{Nb}_4\text{B}_{10}$ fabricated by melt spinning show the following.

1. Kissinger's dependence for amorphous alloy $\text{Fe}_{81}\text{Zr}_5\text{Nb}_4\text{B}_{10}$ may be broken into two intervals differing in slope. The activation energy of the process of crystallization of the alloy amounts to $E_{p11} = 464.9$ kJ/mole for the heating rates of 7–15 K/min and to $E_{p12} = 278.5$ kJ/mole for the heating rates of 15–30 K/min. The value of E_{p11} corresponds to formation of crystallization centers of an α -Mn-type phase in the melt; E_{p12} corresponds to formation of phase α -Fe. For the amorphous alloy $\text{Fe}_{40.5}\text{Co}_{40.5}\text{Zr}_5\text{Nb}_4\text{B}_{10}$ the activation energy of the process of crystallization $E_{p2} = 424$ kJ/mole.

2. The primary products of crystallization of amorphous alloy $\text{Fe}_{81}\text{Zr}_5\text{Nb}_4\text{B}_{10}$ are an α -Mn-type phase and an α -Fe-type phase. Crystallization of alloy $\text{Fe}_{40.5}\text{Co}_{40.5}\text{Zr}_5\text{Nb}_4\text{B}_{10}$ yields only an α -Fe(Co) phase.

3. Variation of the coercivity H_c as a function of the annealing temperature differs considerably for the two alloys studied. The coercivity H_c of alloy $\text{Fe}_{81}\text{Zr}_5\text{Nb}_4\text{B}_{10}$ varies in a complex manner and attains a maximum value after annealing at 873 K. The coercivity of alloy $\text{Fe}_{40.5}\text{Co}_{40.5}\text{Zr}_5\text{Nb}_4\text{B}_{10}$ first decreases and then grows with elevation of the annealing temperature starting with 823 K.

The work has been funded by the Technology Studying Project of "13th five-year" Office of Education of the Jilin Province (No. JJKH20170375KJ) and Graduate Innovative Research Program of the Jilin Normal University (No. 1201611).

REFERENCES

1. S. N. Jiang, J. M. Lei, M. G. Zhang, and M. W. Jia, *Electr. Comp. Mater.*, **28**, 30 (2009).
2. F. L. Kong, C. T. Chang, A. Inoue, et al., *J. Alloys Compd.*, **615**, 163 (2014).
3. Y. Han, F. Kong, C. Chang, et al., *J. Mater. Res.*, **30**, 547 (2015).
4. D. Shen, Y. Wang, G. Xing, et al., *Metall. Mater. Trans. A*, **29**, 149 (1998).
5. T. Patel Ashmi and A. Pratap, *J. Therm. Anal. Calor.*, **107**, 159 (2012).
6. L. Tang, K. Peng, Y. Wu, and W. Zhang, *J. Alloys Compd.*, **695**, 2136 (2017).
7. P. G. Boswell, *J. Mater. Sci.*, **15**, 926 (1980).
8. M. J. Starink, *Thermochim. Acta*, **404**, 163 (2003).
9. H. E. Kissinger, *Bureau of Standards*, **57**, 217 (1956).
10. L. H. Kong, Y. L. Gao, T. T. Song, et al., *Thermochim. Acta*, **522**, 166 (2001).

11. W. Q. Yu, Y. M. Sun, and Z. Hua, *Appl. Surf. Sci.*, **257**, 9733 (2011).
12. H. Huang, G. Shao, and P. Tsakirooulos, *J. Alloys Compd.*, **459**, 185 (2008).
13. Y. C. Zhou and Q. J. Zhang, *Adv. Mater. Res.*, **299**, 584 (2011).
14. A. Wang, H. Men, C. L. Zhao, et al., *Sci. Adv. Mater.*, **7**, 2721 (2015).
15. M. Imafuku, S. Sato, H. Loshiba, et al., *Scr. Mater.*, **44**, 2369 (2001).
16. W. Q. Yu, H. Q. Zeng, Y. M. Sun, et al., *Phys. Lett. A*, **381**, 1573 (2018).
17. T. Nagase and Y. Umakoshi, *ISIJ Int.*, **46**, 1371 (2006).
18. E. Illeková, P. Švec, and M. Miglierini, *J. Non-Cryst. Solids*, **353**, 3342 (2007).
19. A. Takeuchi and A. Inoue, *Mater. Trans.*, **46**, 2817 (2005).
20. Y. M. Sun, B. Zuo, D. Wang, et al., *Acta Phys. Polonica A*, **124**, 685 (2013).
21. S. Ahmadi, H. R. Shahverdi, and S. S. Saremi, *J. Mater. Sci. Technol.*, **27**, 735 (2011).
22. Y. M. Sun, W. Q. Yu, D. Long, et al., *Modern Phys. Lett. B*, **29**, 358 (2015).